

# **Toward a Genome Scale Dynamic Model of Cell-Free Protein Synthesis in *Escherichia coli***

Nicholas Horvath, Michael Vilkhovoy, Joseph Wayman, Kara Calhoun<sup>1</sup>, James Swartz<sup>1</sup> and Jeffrey D. Varner\*

Robert Frederick Smith School of Chemical and Biomolecular Engineering  
Cornell University, Ithaca NY 14853

<sup>1</sup>School of Chemical Engineering  
Stanford University, Stanford, CA 94305

**Running Title:** Dynamic modeling of cell-free protein synthesis

**To be submitted:** *Scientific Reports*

\*Corresponding author:

Jeffrey D. Varner,

Professor, Robert Frederick Smith School of Chemical and Biomolecular Engineering,  
244 Olin Hall, Cornell University, Ithaca NY, 14853

Email: [jdv27@cornell.edu](mailto:jdv27@cornell.edu)

Phone: (607) 255 - 4258

Fax: (607) 255 - 9166

## Abstract

Cell-free protein expression systems have become widely used in systems and synthetic biology. In this study, we developed an ensemble of dynamic *E. coli* cell-free protein synthesis (CFPS) models. Model parameters were estimated from measurements of glucose, organic acids, energy species, amino acids and the protein product, chloramphenicol acetyltransferase (CAT). The ensemble described the training data, with the exception of some of the amino acid dynamics. To gauge the performance of the cell-free reaction, we compared the observed CAT carbon yield, with the maximum theoretical CAT carbon yield calculated using sequence specific flux balance analysis. The observed CAT yield was 45% of the maximum theoretical yield, suggesting CAT production could be further optimized. The metabolic flux distribution predicted by the dynamic model and flux balance analysis were significantly different. The ensemble of dynamic models predicted the majority of carbon flux was routed through glycolysis and the TCA cycle, while flux balance analysis predicted significant flux through the Entner-Doudoroff pathway. Local and global sensitivity analysis suggested CAT production was most sensitive to parameters and initial conditions directly associated with CAT synthesis, as well as GTP/GMP synthesis, amino acid synthesis, and to a lesser extent amino acid initial conditions. On the other hand, CAT production was robust to allosteric control parameters and the initial conditions of glucose and oxygen. Taken together, we presented the first dynamic model of *E. coli* cell-free protein synthesis. This study provides a foundation for genome-scale, dynamic modeling of cell-free *E. coli* protein synthesis.

**Keywords:** Biochemical engineering, systems biology, cell-free protein synthesis

## 1 Introduction

2 Cell-free systems offer many advantages for the study, manipulation and modeling of  
3 metabolism compared to *in vivo* processes. Central amongst these advantages is direct  
4 access to metabolites and the microbial biosynthetic machinery without the interference of  
5 a cell wall. This allows us to control as well as interrogate the chemical environment while  
6 the biosynthetic machinery is operating, potentially at a fine time resolution. Second,  
7 cell-free systems also allow us to study biological processes without the complications  
8 associated with cell growth. Cell-free protein synthesis (CFPS) systems are arguably the  
9 most prominent examples of cell-free systems used today [1]. However, CFPS is not new;  
10 CFPS in crude *E. coli* extracts has been used since the 1960s to explore fundamentally  
11 important biological mechanisms [2, 3]. Today, cell-free systems are used in a variety of  
12 applications ranging from therapeutic protein production [4] to synthetic biology [5]. Inter-  
13 estingly, many of the challenges confronting genome-scale kinetic modeling can poten-  
14 tially be overcome in a cell-free system. For example, there is no complex transcriptional  
15 regulation to consider, transient metabolic measurements are easier to obtain, and we  
16 no longer have to consider cell growth. Thus, cell-free operation holds several significant  
17 advantages for model development, identification and validation. Theoretically, genome-  
18 scale cell-free kinetic models may be possible for industrially important organisms, such  
19 as *E. coli* or *B. subtilis*, if a simple, tractable framework for integrating allosteric regulation  
20 with enzyme kinetics can be formulated.

21 Mathematical modeling has long contributed to our understanding of metabolism. Decades  
22 before the genomics revolution, mechanistically, structured metabolic models arose from  
23 the desire to predict microbial phenotypes resulting from changes in intracellular or extra-  
24 cellular states [6]. The single cell *E. coli* models of Shuler and coworkers pioneered the  
25 construction of large-scale, dynamic metabolic models that incorporated multiple, regu-  
26 lated catabolic and anabolic pathways constrained by experimentally determined kinetic

parameters [7]. Shuler and coworkers generated many single cell kinetic models, including single cell models of eukaryotes [8, 9], minimal cell architectures [10], as well as DNA sequence based whole-cell models of *E. coli* [11]. Conversely, highly abstracted kinetic frameworks, such as the cybernetic framework, represented a paradigm shift, viewing cells as growth-optimizing strategists [12]. Cybernetic models have been highly successful at predicting metabolic choice behavior, e.g., diauxie behavior [13], steady-state multiplicity [14], as well as the cellular response to metabolic engineering modifications [15]. Unfortunately, traditional, fully structured cybernetic models also suffer from an identifiability challenge, as both the kinetic parameters and an abstracted model of cellular objectives must be estimated simultaneously. However, recent cybernetic formulations from Ramkrishna and colleagues have successfully treated this identifiability challenge through elementary mode reduction [16, 17].

In the post genomics world, large-scale stoichiometric reconstructions of microbial metabolism popularized by static, constraint-based modeling techniques such as flux balance analysis (FBA) have become standard tools [18]. Since the first genome-scale stoichiometric model of *E. coli*, developed by Edwards and Palsson [19], well over 100 organisms, including industrially important prokaryotes such as *E. coli* [20] or *B. subtilis* [21], are now available [22]. Stoichiometric models rely on a pseudo-steady-state assumption to reduce unidentifiable genome-scale kinetic models to an underdetermined linear algebraic system, which can be solved efficiently even for large systems. Traditionally, stoichiometric models have also neglected explicit descriptions of metabolic regulation and control mechanisms, instead opting to describe the choice of pathways by prescribing an objective function on metabolism. Interestingly, similar to early cybernetic models, the most common metabolic objective function has been the optimization of biomass formation [23], although other metabolic objectives have also been estimated [24]. Recent advances in constraint-based modeling have overcome the early shortcomings of

the platform, including capturing metabolic regulation and control [25]. Thus, modern constraint-based approaches have proven extremely useful in the discovery of metabolic engineering strategies and represent the state of the art in metabolic modeling [26, 27]. However, genome-scale kinetic models of industrial important organisms such as *E. coli* have yet to be constructed.

In this study, we developed an ensemble of *E. coli* cell-free protein synthesis (CFPS) models using the hybrid cell-free modeling approach of Wayman et al [REFHERE]. Model parameters were estimated from measurements of glucose, organic acids, energy species, amino acids and the protein product, chloramphenicol acetyltransferase (CAT). The ensemble described the training data, with the exception of some of the amino acid dynamics. To gauge the performance of the cell-free reaction, we compared the observed CAT carbon yield, with the maximum theoretical CAT carbon yield calculated using sequence specific flux balance analysis. The observed CAT yield was 45% of the maximum theoretical yield, suggesting CAT production could be further optimized. The metabolic flux distribution predicted by the dynamic model and flux balance analysis were significantly different. The ensemble of dynamic models predicted the majority of carbon flux was routed through glycolysis and the TCA cycle, while flux balance analysis predicted significant flux through the Entner-Doudoroff pathway. Local and global sensitivity analysis suggested CAT production was most sensitive to parameters and initial conditions directly associated with CAT synthesis, as well as GTP/GMP synthesis, amino acid synthesis, and to a lesser extent amino acid initial conditions. On the other hand, CAT production was robust to allosteric control parameters and the initial conditions of glucose and oxygen. Taken together, we presented the first dynamic model of *E. coli* cell-free protein synthesis. We integrated traditional kinetics with a logical rule-based description of allosteric control to simulate a comprehensive CFPS dataset. This study provides a foundation for genome-scale, dynamic modeling of cell-free *E. coli* protein synthesis.

## Results

**Estimation of an ensemble of cell-free protein synthesis models.** We used the hybrid cell-free modeling framework of Wayman et al. to simulate the production of a model protein [REFHERE]. The cell-free *E. coli* metabolic model was constructed by removing the growth-associated processes from the model of Palsson and coworkers [19], and by adding reactions for the synthesis of chloramphenicol acetyltransferase (CAT), a model protein for which we have a comprehensive training dataset [28]. Thus, the model described core central carbon metabolism (glycolysis, pentose phosphate, Enter-Doudoroff, TCA cycle), as well as the synthesis of energy species, amino acids biosynthesis and degradation, and biosynthesis of the CAT protein. An ensemble of model parameters was estimated from dynamic measurements of glucose, CAT, organic acids (pyruvate, lactate, acetate, succinate, malate), energy species (A(x)P, G(x)P, C(x)P, U(x)P), and 18 of the 20 proteinogenic amino acids. We generated an ensemble of  $N = 18,000$  parameter sets by minimizing the error between the training dataset and the metabolite concentrations predicted by the model. We defined the set with the lowest error value as the best-fit parameter set. [STATISTICS ON PARAMETERS].

The ensemble of models captured the time evolution of cell-free CAT biosynthesis (Fig. 1 - 3). Glucose was exhausted with 3 hr [FILL ME IN]. The ensemble also captured the energy species dynamics, particularly the overall energy total (Fig. 1, top) and the totals by base . The ensemble and the best-fit set also predict some of the amino acid measurements, while failing to predict others (Fig. 3). the central carbon metabolism, including glucose uptake, CAT production, and the dynamics of the organic acid intermediates . Allosteric control is important to the dynamics of the organic acid intermediates, as without it several of the measurements are not captured by the ensemble or the best-fit set (Fig. 1, bottom). This is likely due to a structural deficiency in the model; in some cases, the consumption of an amino acid through CAT synthesis is not enough to ex-

plain the decrease shown in the data, and there are no other reactions that consume it. Thus, a more comprehensive biological description is needed to fully explain amino acid dynamics.

**Sensitivity analysis** We performed a local sensitivity analysis to determine the network reactions with the greatest effect on protein production and overall system state. CAT production was most sensitive to the CAT synthesis reaction, oxidative phosphorylation activity, and alanine synthesis, as well as various reactions in glycolysis, the TCA cycle, and amino acid synthesis and degradation.

**Maximum theoretical CAT yield showed CFPS can be optimized.** We calculated the carbon yield of CAT production for our experimental data and our best-fit parameter set as a function of the initial and final concentrations and the carbon numbers of CAT, glucose, and amino acids. The experimental data displayed a CAT yield of 0.0865, while the best-fit parameter set displayed a CAT yield of 0.0871. While the model ensemble described the experimental data, it was unclear whether the performance of the CFPS system was optimal. To address this question, we used ssFBA in combination with the cell-free metabolic network and a detailed promoter model under a T7 polymerase to compute the maximum theoretical carbon yield. However, we first validated the ssFBA approach by comparing an ensemble of simulated versus measured concentrations of CAT over a one hour period (Fig. 7A). The ensemble of 100 sets captured the CAT concentration profile which was generated by sampling RNA polymerase levels, ribosome levels and elongation rates in a physiological range. We then used sequence-specific FBA to calculate a theoretical maximum CAT yield under three different cases: unconstrained, constrained by transcription/translation rates, and constrained by transcription/translation rates and measurements (Fig. 7B). The theoretical maximum carbon yield of CAT was  $0.35 \pm 0.006$  for an unconstrained case and  $0.225 \pm 0.03$  for the transcription and translation constrained case. Thus, we showed that our experimental dataset and best-fit pa-

parameter set were each producing CAT at 25% of the theoretical maximum and 38% of a theoretical physiological case. Whereas, the case constrained by experimental data had a carbon yield of  $0.062 \pm 0.02$ , similar to the experimental yield. In comparing the flux distributions between the unconstrained and constrained cases (Fig. 8), the constrained cases heavily utilize the first step in the pentose phosphate pathway to generate NADPH. The majority of the flux continues through the Entner–Doudoroff pathway whereas in the unconstrained case, the majority of flux travels through glycolysis. In all cases, the energy source comes from oxidative phosphorylation with some from the citric acid cycle. Whereas, in just the TX/TL case, there is a high flux through fumerate dehydrogenase from aspartic acid uptake. In the unconstrained and most constrained case, we see a mixture of acetate and lactate accumulation. This shows the system is producing NADH through lactate dehydrogenase as well as through pyridine nucleotide transhydrogenase (*pntAB*) to supply enough NADH for oxidative phosphorylation. As a result, high oxidative phosphorylation activity relative to our cell free system leads to an acetate overflow. This suggests that there is potential for increasing CAT production by reducing this diversion of carbon. To simulate potential knockouts, we constrained the specific glucose and amino acid uptake rates to the same values as simulated with no knockouts. In an ssFBA simulation with constrained TX/TL rates, knocking out the *gnd* reaction decreases flux of acetate production but increases flux through *pntAB* which is responsible for regenerating NADPH. The simulation showed carbon was diverted towards lactate, however since CAT production is constrained by the translation rate, we expected there to be no increase in CAT production. The decrease in acetate production is a promising result to increase CAT yield. A second simulation with a knockout of *gnd* and phosphate acetyltransferase, showed carbon being diverted towards lactate and succinate, however it required a higher flux through oxidative phosphorylation and the TCA cycle to meet the energetic needs of the system.



## Discussion

In this study, we developed an ensemble of *E. coli* cell-free protein synthesis (CFPS) models using the hybrid cell-free modeling approach of Wayman et al [REFHERE]. Model parameters were estimated from measurements of glucose, organic acids, energy species, amino acids and the protein product, chloramphenicol acetyltransferase (CAT). The ensemble described the training data, with the exception of some of the amino acid dynamics. To gauge the performance of the cell-free reaction, we compared the observed CAT carbon yield, with the maximum theoretical CAT carbon yield calculated using sequence specific flux balance analysis. The observed CAT yield was 25% of the maximum theoretical yield, suggesting CAT production could be further optimized. The metabolic flux distribution predicted by the dynamic model and flux balance analysis were significantly different. The ensemble of dynamic models predicted the majority of carbon flux was routed through glycolysis and the TCA cycle, while flux balance analysis predicted significant flux through the Entner-Doudoroff pathway. Local and global sensitivity analysis suggested CAT production was most sensitive to parameters and initial conditions directly associated with CAT synthesis, as well as GTP/GMP synthesis, amino acid synthesis, and to a lesser extent amino acid initial conditions. On the other hand, CAT production was robust to allosteric control parameters and the initial conditions of glucose and oxygen.

In comparing the theoretical maximum carbon yield of CAT from ssFBA predictions to the kinetic model and experimental measurements, suggests that there is potential for increasing CAT yield in CFPS as well as CFPS performance. The theoretical maximum yield of CAT was 0.35 for an unconstrained case and 0.225 for a transcription/translation constrained case. Knockouts of *gnd* and phosphate acetyltransferase, show carbon can be diverted away from acetate and potentially towards CAT or other proteins of interest expressed in CFPS. The other limitations to address in CFPS would be to enhance the transcription and translation rates since the protein of interest to be expressed is ultimately

183 bounded by these kinetic rates. Li et al. have increased productivity of firefly luciferase by  
184 5-fold in CFPS systems by adding and adjusting factors that affect transcription and trans-  
185 lation such as elongation factors, ribosome recycling factor, release factors, chaperones,  
186 BSA and tRNAs [29]. Underwood et al. has also shown the increase in ribosome levels  
187 does not significantly increase protein yields and rates, however adding elongation factors  
188 increased yields by 23% at 30 minutes[30]. In addition to improving CFPS performance,  
189 Jewett et al. has showed that oxidative phosphorylation operates in cell-free systems and  
190 knocking out oxidative phosphorylation reactions is detrimental to protein yield [31]. How-  
191 ever, it is inconclusive how much oxidative phosphorylation activity there is compared to  
192 *in vivo* systems and both of our models suggest oxidative phosphorylation is vital to CAT  
193 production. Thus, this is a potential place for improvement to optimize CFPS for better  
194 performance and protein yield.

195 The cell-free model ensemble described the training data with the exception of some  
196 of the amino acids. Specifically, adding more reactions that consume amino acids would  
197 improve the model's ability to predict those that show a decrease in the experimental data.  
198 Also, including specific transcription and translation steps for CAT would allow us to more  
199 accurately model the complexity and the resource cost of protein synthesis. Another area  
200 for future work is to more thoroughly sample parameter space. For the metabolites in the  
201 dataset, initial conditions were fixed at the initial data values. All other parameters were  
202 varied in a manner so as to best fit the dataset. However, the resulting ensemble may not  
203 represent every biological or practical possibility. In a different region of parameter space,  
204 the system could behave differently, including the flux distribution through the network,  
205 the accuracy and spread of ensemble fits, the relative sensitivities, and the yield as a per-  
206 centage of the theoretical maximum. Testing the model under a variety of conditions could  
207 strengthen or challenge the findings of this study. Further experimentation could also be  
208 used to gain a deeper understanding of model performance under a variety of conditions.

Specifically, CAT production performed in the absence of amino acids could inform the system's ability to manufacture them, while experimentation in the absence of glucose or oxygen could shed light on how important they are to protein synthesis, and under which conditions. Finally, the approach should be extended to other protein products. CAT is only a test protein used for model identification; the modeling framework, and to some extent the parameter values, should be protein agnostic. An important extension of this study would be to apply its insights to other protein applications, where possible.

## Materials and Methods

**Formulation and solution of the model equations** We used ordinary differential equations (ODEs) to model the time evolution of metabolite ( $x_i$ ) and scaled enzyme abundance ( $\epsilon_i$ ) in hypothetical cell-free metabolic networks:

$$\frac{dx_i}{dt} = \sum_{j=1}^{\mathcal{R}} \sigma_{ij} r_j(\mathbf{x}, \epsilon, \mathbf{k}) \quad i = 1, 2, \dots, \mathcal{M} \quad (1)$$

$$\frac{d\epsilon_i}{dt} = -\lambda_i \epsilon_i \quad i = 1, 2, \dots, \mathcal{E} \quad (2)$$

where  $\mathcal{R}$  denotes the number of reactions,  $\mathcal{M}$  denotes the number of metabolites and  $\mathcal{E}$  denotes the number of enzymes in the model. The quantity  $r_j(\mathbf{x}, \epsilon, \mathbf{k})$  denotes the rate of reaction  $j$ . Typically, reaction  $j$  is a non-linear function of metabolite and enzyme abundance, as well as unknown kinetic parameters  $\mathbf{k}$  ( $\mathcal{K} \times 1$ ). The quantity  $\sigma_{ij}$  denotes the stoichiometric coefficient for species  $i$  in reaction  $j$ . If  $\sigma_{ij} > 0$ , metabolite  $i$  is produced by reaction  $j$ . Conversely, if  $\sigma_{ij} < 0$ , metabolite  $i$  is consumed by reaction  $j$ , while  $\sigma_{ij} = 0$  indicates metabolite  $i$  is not connected with reaction  $j$ . Lastly,  $\lambda_i$  denotes the scaled enzyme degradation constant. The system material balances were subject to the initial conditions  $\mathbf{x}(t_o) = \mathbf{x}_o$  and  $\epsilon(t_o) = 1$  (initially we have 100% cell-free enzyme abundance).

The reaction rate was written as the product of a kinetic term ( $\bar{r}_j$ ) and a control term ( $v_j$ ),  $r_j(\mathbf{x}, \mathbf{k}) = \bar{r}_j v_j$ . In this study, we used either saturation or mass action kinetics. The control term  $0 \leq v_j \leq 1$  depended upon the combination of factors which influenced rate process  $j$ . For each rate, we used a rule-based approach to select from competing control factors. If rate  $j$  was influenced by  $1, \dots, m$  factors, we modeled this relationship as  $v_j = \mathcal{I}_j(f_{1j}(\cdot), \dots, f_{mj}(\cdot))$  where  $0 \leq f_{ij}(\cdot) \leq 1$  denotes a regulatory transfer function quantifying the influence of factor  $i$  on rate  $j$ . The function  $\mathcal{I}_j(\cdot)$  is an integration rule which maps the output of regulatory transfer functions into a control variable. Each regulatory

transfer function took the form:

$$f_{ij}(\mathcal{Z}_i, k_{ij}, \eta_{ij}) = k_{ij}^{\eta_{ij}} \mathcal{Z}_i^{\eta_{ij}} / (1 + k_{ij}^{\eta_{ij}} \mathcal{Z}_i^{\eta_{ij}}) \quad (3)$$

where  $\mathcal{Z}_i$  denotes the abundance factor  $i$ ,  $k_{ij}$  denotes a gain parameter, and  $\eta_{ij}$  denotes a cooperativity parameter. In this study, we used  $\mathcal{I}_j \in \{mean\}$  [? ]. If a process has no modifying factors,  $v_j = 1$ . We used multiple saturation kinetics to model the reaction term  $\bar{r}_j$ :

$$\bar{r}_j = k_j^{max} \epsilon_i \left( \prod_{s \in m_j^-} \frac{x_s}{K_{js} + x_s} \right) \quad (4)$$

where  $k_j^{max}$  denotes the maximum rate for reaction  $j$ ,  $\epsilon_i$  denotes the scaled enzyme activity which catalyzes reaction  $j$ , and  $K_{js}$  denotes the saturation constant for species  $s$  in reaction  $j$ . The product in Equation (4) was carried out over the set of *reactants* for reaction  $j$  (denoted as  $m_j^-$ ).

We added regulation to the network as informed by literature, for a total of 17 interactions. PEP was modeled as an inhibitor for phosphofructokinase [32, 33], PEP carboxykinase [32], PEP synthetase [32, 34], isocitrate dehydrogenase [32, 35], and isocitrate lyase/malate synthase [32, 35, 36], and as an activator for fructose-biphosphatase [32, 37–39]. AKG was modeled as an inhibitor for citrate synthase [32, 40, 41] and isocitrate lyase/malate synthase [32, 36]. 3PG was modeled as an inhibitor for isocitrate lyase/malate synthase [32, 36]. FDP was modeled as an activator for pyruvate kinase [32, 42] and PEP carboxylase [32, 43]. Pyruvate was modeled as an inhibitor for pyruvate dehydrogenase [32, 44, 45] and as an activator for lactate dehydrogenase [46]. Acetyl CoA was modeled as an inhibitor for malate dehydrogenase [32].

**Generation of model ensemble** We generated an ensemble of 100 diverse parameter sets via a Markov chain Monte Carlo random walk. Beginning with a single parameter

258 set as a starting point, we calculated its cost function, equal to the sum-squared-error  
 259 between experimental data and model predictions:

$$cost = \sum_{i=1}^{\mathcal{D}} \left( w_i \sum_{j=1}^{\mathcal{T}_i} abs \left( x_{ij}^{data} - x_i^{sim}|_{t(j)} \right) \right) \quad (5)$$

260 where  $\mathcal{D}$  denotes the number of datasets,  $w_i$  denotes the weight of the  $i$ th dataset,  $\mathcal{T}_i$   
 261 denotes the number of timepoints in the  $i$ th dataset,  $t(j)$  denotes the  $j$ th timepoint,  $x_{ij}^{data}$   
 262 denotes the value of the  $i$ th dataset at the  $j$ th timepoint, and  $x_i^{sim}|_{t(j)}$  denotes the sim-  
 263 ulated value of the metabolite corresponding to the  $i$ th dataset, interpolated to the  $j$ th  
 264 timepoint. We then perturbed model parameters:

$$k_i^{new} = k_i * exp(a r_i) \quad i = 1, 2, \dots, \mathcal{P} \quad (6)$$

265 where  $\mathcal{P}$  denotes the number of parameters, equal to 815, which includes 163 rate con-  
 266 stants, 163 enzyme degradation rate constants, 455 saturation constants, and 34 control  
 267 parameters,  $k_i^{new}$  denotes the new value of the  $i$ th parameter,  $k_i$  denotes the current value  
 268 of the  $i$ th parameter,  $a$  denotes a distribution variance, and  $r_i$  denotes a random sample  
 269 from the normal distribution. For each newly generated parameter set, we re-solved the  
 270 balance equations and calculated the cost function. All sets with a lower cost than the  
 271 previous set, and some with higher cost, were added to the ensemble. After generating  
 272 12,437 sets, we selected 100 sets with minimal correlation to each other so as to avoid  
 273 over-sampling any region of parameter space. The original 12,437-set ensemble had  
 274 a [mean,median,maximum] Pearson correlation coefficient [REFERENCE NEEDED?] of  
 275 [?] between pairs of sets; the 100-set ensemble had a [mean,median,maximum] Pearson  
 276 correlation coefficient of [?] between pairs of sets.

**Sensitivity analysis** We determined the reactions most important to protein production by computing the local sensitivity of CAT concentration to each rate constant in the network. Each sensitivity index was formulated as:

$$S_{ij} = \text{norm}(CAT(p_i, p_j, t) - CAT(\alpha * p_i, \alpha * p_j, t)) \quad i, j = 1, 2, \dots \mathcal{P} \quad (7)$$

where  $S_{ij}$  denotes the sensitivity of CAT production to the  $i$ th and  $j$ th parameters,  $CAT(p_i, p_j, t)$  denotes CAT concentration as a function of time and the  $i$ th and  $j$ th parameters,  $\alpha$  denotes the perturbation factor, equal to 1.01, and  $\mathcal{P}$  denotes the number of rate constants, equal to 163. In calculating the pairwise sensitivities, each parameter was perturbed by 1%; first-order sensitivities ( $i = j$ ) were subject to two 1% perturbations, equivalent to a perturbation of 2.01%.

**Sequence specific FBA and calculation of CAT yield** The yield on CAT production was calculated for each case as a ratio of carbon produced as CAT to carbon consumed as reactants (glucose and amino acids):

$$Yield = \frac{\Delta CAT \ C_{CAT}}{\sum_{i=1}^{\mathcal{R}} \max(\Delta m_i, 0) \ C_{m_i}} \quad (8)$$

where  $\Delta CAT$  denotes the amount of CAT produced,  $C_{CAT}$  denotes carbon number of CAT,  $\mathcal{R}$  denotes the number of reactants,  $\Delta m_i$  denotes the amount of the  $i$ th reactant consumed, never allowed to be negative, and  $C_{m_i}$  denotes the carbon number of the  $i$ th reactant. Because no data was available for arginine or glutamate, these reactants were left out of all three calculations. In the experimental case and the best-fit set case, yield was calculated by setting  $\Delta CAT$  equal to the final minus the initial CAT concentration and setting  $\Delta m_i$  equal to the initial minus the final reactant concentration. The theoretical yield was calculated using flux balance analysis (FBA) with a sequence-specific based

297 analysis on CAT. The sequence specific FBA [47] problem was formulated as:

$$\max_{\mathbf{w}} (w_{obj} = \boldsymbol{\theta}^T \mathbf{w})$$

$$\text{Subject to : } \mathbf{S}\mathbf{w} = \mathbf{0}$$

$$\alpha_i \leq w_i \leq \beta_i \quad i = 1, 2, \dots, \mathcal{R}$$

298 where  $\mathbf{S}$  denotes the stoichiometric matrix,  $\mathbf{w}$  denotes the unknown flux vector,  $\boldsymbol{\theta}$  de-  
 299 notes the objective selection vector and  $\alpha_i$  and  $\beta_i$  denote the lower and upper bounds  
 300 on flux  $w_i$ , respectively. The objective  $w_{obj}$  was to maximize the specific rate of CAT for-  
 301 mation. The specific glucose uptake rate was constrained to allow a maximum flux of 40  
 302 mM/hr according to experimental data; the specific amino acid uptake rates were bound  
 303 to allow a maximum flux of 30 mM/hr, but did not reach this maximum flux. The tran-  
 304 scription and translation template reactions were added to the metabolic network and are  
 305 based off sequence specific analysis [47] involving transcription initiaion, transcription,  
 306 mRNA degradation, translation initiation, translation, and tRNA charging. The flux bal-  
 307 ance analysis problem was solved using the GNU Linear Programming Kit (v4.52) [48].  
 308 The solution flux vector was used to calculate the theoretical carbon yield of CAT. Glucose,  
 309 oxygen, and amino acids were modeled as being imported into the system, whereas CAT  
 310 synthesis and metabolite byproduct formation was modeled as an export from the sys-  
 311 tem. The rest of the network followed a pseudo steady-state asusmption where all other  
 312 metabolites were not allowed to accumulate; thus, the network could be solved by linear  
 313 programming.

314 The transcription rate was constrained as:

$$w_{tx} = RNAP \frac{v_{RNAP}}{l_{mRNA}} \left( \frac{Gene}{km + Gene} \right) P$$

315 where  $RNAP$  is the concentration of RNA polymerase,  $v_{RNAP}$  is the elongation rate (nu-



cleotides/hr) by the RNA polymerase,  $l_{mRNA}$  is the number of nucleotides in the mRNA,  $Gene$  is the gene concentration,  $km$  is the plasmid saturation coefficient, and  $P$  is the promoter activity. The mRNA and protein sequence of CAT was determined from literature.

The promoter activity was formulated following Moon et al. for synthetic circuits as:

$$P = \frac{K_1}{1 + K_1}$$

where  $K_1$  represents the state of T7 RNA polymerase binding.

The translation rate was constrained as:

$$w_{tl} = K_P Ribo \frac{v_{Ribo}}{l_{protein}} [mRNA_{ss}]$$

where  $K_P$  is the polysome amplification constant,  $Ribo$  is the ribosome concentration,  $v_{Ribo}$  is the elongation rate (amino acids/hr) of the ribosome,  $l_{protein}$  is the number of amino acids in the protein of interest, and  $mRNA_{ss}$  is the mRNA concentration at steady state determined by the transcription rate divided by the degradation rate of mRNA.

An ensemble of 100 sets of flux distributions was calculated for three different cases, unconstrained, constrained by transcription and translation (TX/TL) rates, and constrained by TX/TL rates and experimental data. For the unconstrained case, all rates were left unbounded, except for the specific glucose uptake rate. An ensemble of flux distributions was calculated by randomly sampling the maximum specific glucose uptake rate from 30 to 40 mM/hr determined from experimental data. For the case constrained by TX/TL rates, an ensemble was generated by randomly sampling RNAP polymerase levels, ribosome levels, and elongation rates in a physiological range determined from literature. RNA polymerase levels were sampled between 60 and 80 nM, ribosome levels between 7 and 16  $\mu$ M, the elongation rate by RNA polymerase between 20 and 30 nts/sec, and the elongation rate by ribosomes between 1.5 and 3 AA/sec [30, 49]. For the case constrained

337 by TX/TL rates and experimental data, an ensemble was generated by randomly sam-  
338 pling RNAP polymerase levels, ribosome levels, and elongation rates in a physiological  
339 range determined from literature. The lower and upper bound constraints were randomly  
340 sampled in the physiological range of the experimental noise where data was available,  
341 except for CAT flux, which was determined from the transcription and translation rates.

## **Funding**

This study was supported by a National Science Foundation Graduate Research Fellowship (DGE-1333468) to N.H and by an award from the US Army and Systems Biology of Trauma Induced Coagulopathy (W911NF-10-1-0376) to J.V for the support of M.V.

## References

1. Jewett MC, Calhoun KA, Voloshin A, Wu JJ, Swartz JR (2008) An integrated cell-free metabolic platform for protein production and synthetic biology. *Mol Syst Biol* 4: 220.
2. Matthaei JH, Nirenberg MW (1961) Characteristics and stabilization of dnaase-sensitive protein synthesis in e. coli extracts. *Proc Natl Acad Sci U S A* 47: 1580-8.
3. Nirenberg MW, Matthaei JH (1961) The dependence of cell-free protein synthesis in e. coli upon naturally occurring or synthetic polyribonucleotides. *Proc Natl Acad Sci U S A* 47: 1588-602.
4. Lu Y, Welsh JP, Swartz JR (2014) Production and stabilization of the trimeric influenza hemagglutinin stem domain for potentially broadly protective influenza vaccines. *Proc Natl Acad Sci U S A* 111: 125-30.
5. Hodgman CE, Jewett MC (2012) Cell-free synthetic biology: thinking outside the cell. *Metab Eng* 14: 261-9.
6. Fredrickson AG (1976) Formulation of structured growth models. *Biotechnol Bioeng* 18: 1481-6.
7. Domach MM, Leung SK, Cahn RE, Cocks GG, Shuler ML (1984) Computer model for glucose-limited growth of a single cell of escherichia coli b/r-a. *Biotechnol Bioeng* 26: 203-16.
8. Steinmeyer D, Shuler M (1989) Structured model for *Saccharomyces cerevisiae*. *Chem Eng Sci* 44: 2017 - 2030.
9. Wu P, Ray NG, Shuler ML (1992) A single-cell model for cho cells. *Ann N Y Acad Sci* 665: 152-87.
10. Castellanos M, Wilson DB, Shuler ML (2004) A modular minimal cell model: purine and pyrimidine transport and metabolism. *Proc Natl Acad Sci U S A* 101: 6681-6.
11. Atlas JC, Nikolaev EV, Browning ST, Shuler ML (2008) Incorporating genome-wide

dna sequence information into a dynamic whole-cell model of escherichia coli: application to dna replication. IET Syst Biol 2: 369-82.

12. Dhurjati P, Ramkrishna D, Flickinger MC, Tsao GT (1985) A cybernetic view of microbial growth: modeling of cells as optimal strategists. Biotechnol Bioeng 27: 1-9.

13. Kompala DS, Ramkrishna D, Jansen NB, Tsao GT (1986) Investigation of bacterial growth on mixed substrates: experimental evaluation of cybernetic models. Biotechnol Bioeng 28: 1044-55.

14. Kim JI, Song HS, Sunkara SR, Lali A, Ramkrishna D (2012) Exacting predictions by cybernetic model confirmed experimentally: steady state multiplicity in the chemostat. Biotechnol Prog 28: 1160-6.

15. Varner J, Ramkrishna D (1999) Metabolic engineering from a cybernetic perspective: aspartate family of amino acids. Metab Eng 1: 88-116.

16. Song HS, Morgan JA, Ramkrishna D (2009) Systematic development of hybrid cybernetic models: application to recombinant yeast co-consuming glucose and xylose. Biotechnol Bioeng 103: 984-1002.

17. Song HS, Ramkrishna D (2011) Cybernetic models based on lumped elementary modes accurately predict strain-specific metabolic function. Biotechnol Bioeng 108: 127-40.

18. Lewis NE, Nagarajan H, Palsson BØ (2012) Constraining the metabolic genotype-phenotype relationship using a phylogeny of in silico methods. Nat Rev Microbiol 10: 291-305.

19. Edwards JS, Palsson BØ (2000) The escherichia coli mg1655 in silico metabolic genotype: its definition, characteristics, and capabilities. Proc Natl Acad Sci U S A 97: 5528-33.

20. Feist AM, Henry CS, Reed JL, Krummenacker M, Joyce AR, et al. (2007) A genome-scale metabolic reconstruction for escherichia coli k-12 mg1655 that accounts for

1260 orfs and thermodynamic information. *Mol Syst Biol* 3: 121.

21. Oh YK, Palsson BØ, Park SM, Schilling CH, Mahadevan R (2007) Genome-scale reconstruction of metabolic network in *Bacillus subtilis* based on high-throughput phenotyping and gene essentiality data. *J Biol Chem* 282: 28791-9.
22. Feist AM, Herrgård MJ, Thiele I, Reed JL, Palsson BØ (2009) Reconstruction of biochemical networks in microorganisms. *Nat Rev Microbiol* 7: 129-43.
23. Ibarra RU, Edwards JS, Palsson BØ (2002) *Escherichia coli* K-12 undergoes adaptive evolution to achieve in silico predicted optimal growth. *Nature* 420: 186-9.
24. Schuetz R, Kuepfer L, Sauer U (2007) Systematic evaluation of objective functions for predicting intracellular fluxes in *Escherichia coli*. *Mol Syst Biol* 3: 119.
25. Hyduke DR, Lewis NE, Palsson BØ (2013) Analysis of omics data with genome-scale models of metabolism. *Mol Biosyst* 9: 167-74.
26. McCloskey D, Palsson BØ, Feist AM (2013) Basic and applied uses of genome-scale metabolic network reconstructions of *Escherichia coli*. *Mol Syst Biol* 9: 661.
27. Zomorodi AR, Suthers PF, Ranganathan S, Maranas CD (2012) Mathematical optimization applications in metabolic networks. *Metab Eng* 14: 672-86.
28. Calhoun KA, Swartz JR (2005) An economical method for cell-free protein synthesis using glucose and nucleoside monophosphates. *Biotechnology Progress* 21: 1146–1153.
29. Li J, Gu L, Aach J, Church GM (2014) Improved cell-free RNA and protein synthesis system. *PLoS ONE* 9: 1-11.
30. Underwood KA, Swartz JR, Puglisi JD (2005) Quantitative polysome analysis identifies limitations in bacterial cell-free protein synthesis. *Biotechnology and Bioengineering* 91: 425–435.
31. Jewett MC, Calhoun KA, Voloshin A, Wu JJ, Swartz JR (2008) An integrated cell-free metabolic platform for protein production and synthetic biology. *Molecular Systems*

Biology 4.

32. Kotte O, Zaugg JB, Heinemann M (2010) Bacterial adaptation through distributed sensing of metabolic fluxes. *Mol Syst Biol* 6: 355.
33. Cabrera R, Baez M, Pereira HM, Caniuguir A, Garratt RC, et al. (2011) The crystal complex of phosphofructokinase-2 of *Escherichia coli* with fructose-6-phosphate: kinetic and structural analysis of the allosteric ATP inhibition. *J Biol Chem* 286: 5774–5783.
34. Chulavatnatol M, Atkinson DE (1973) Phosphoenolpyruvate synthetase from *Escherichia coli*. Effects of adenylate energy charge and modifier concentrations. *J Biol Chem* 248: 2712–2715.
35. Ogawa T, Murakami K, Mori H, Ishii N, Tomita M, et al. (2007) Role of phosphoenolpyruvate in the NADP-isocitrate dehydrogenase and isocitrate lyase reaction in *Escherichia coli*. *J Bacteriol* 189: 1176–1178.
36. MacKintosh C, Nimmo HG (1988) Purification and regulatory properties of isocitrate lyase from *Escherichia coli* ML308. *Biochem J* 250: 25–31.
37. Donahue JL, Bownas JL, Niehaus WG, Larson TJ (2000) Purification and characterization of glpX-encoded fructose 1, 6-bisphosphatase, a new enzyme of the glycerol 3-phosphate regulon of *Escherichia coli*. *J Bacteriol* 182: 5624–5627.
38. Hines JK, Fromm HJ, Honzatko RB (2006) Novel allosteric activation site in *Escherichia coli* fructose-1,6-bisphosphatase. *J Biol Chem* 281: 18386–18393.
39. Hines JK, Fromm HJ, Honzatko RB (2007) Structures of activated fructose-1,6-bisphosphatase from *Escherichia coli*. Coordinate regulation of bacterial metabolism and the conservation of the R-state. *J Biol Chem* 282: 11696–11704.
40. Pereira DS, Donald LJ, Hosfield DJ, Duckworth HW (1994) Active site mutants of *Escherichia coli* citrate synthase. Effects of mutations on catalytic and allosteric properties. *J Biol Chem* 269: 412–417.

- 450 41. Robinson MS, Easom RA, Danson MJ, Weitzman PD (1983) Citrate synthase of Es-  
451 cherichia coli. Characterisation of the enzyme from a plasmid-cloned gene and am-  
452 plification of the intracellular levels. FEBS Lett 154: 51–54.
- 453 42. Zhu T, Bailey MF, Angley LM, Cooper TF, Dobson RC (2010) The quaternary structure  
454 of pyruvate kinase type 1 from Escherichia coli at low nanomolar concentrations.  
455 Biochimie 92: 116–120.
- 456 43. Wohl RC, Markus G (1972) Phosphoenolpyruvate carboxylase of Escherichia coli.  
457 Purification and some properties. J Biol Chem 247: 5785–5792.
- 458 44. Kale S, Arjunan P, Furey W, Jordan F (2007) A dynamic loop at the active center  
459 of the Escherichia coli pyruvate dehydrogenase complex E1 component modulates  
460 substrate utilization and chemical communication with the E2 component. J Biol  
461 Chem 282: 28106–28116.
- 462 45. Arjunan P, Nemeria N, Brunskill A, Chandrasekhar K, Sax M, et al. (2002) Structure of  
463 the pyruvate dehydrogenase multienzyme complex E1 component from Escherichia  
464 coli at 1.85 Å resolution. Biochemistry 41: 5213–5221.
- 465 46. Okino S, Suda M, Fujikura K, Inui M, Yukawa H (2008) Production of D-lactic acid by  
466 Corynebacterium glutamicum under oxygen deprivation. Appl Microbiol Biotechnol  
467 78: 449–454.
- 468 47. Allen TE, Palsson BØ (2003) Sequence-based analysis of metabolic demands for  
469 protein synthesis in prokaryotes. Journal of Theoretical Biology 220: 1 - 18.
- 470 48. (2016). GNU Linear Programming Kit, Version 4.52. URL [http://www.gnu.org/](http://www.gnu.org/software/glpk/glpk.html)  
471 [software/glpk/glpk.html](http://www.gnu.org/software/glpk/glpk.html).
- 472 49. Garamella J, Marshall R, Rustad M, Noireaux V .



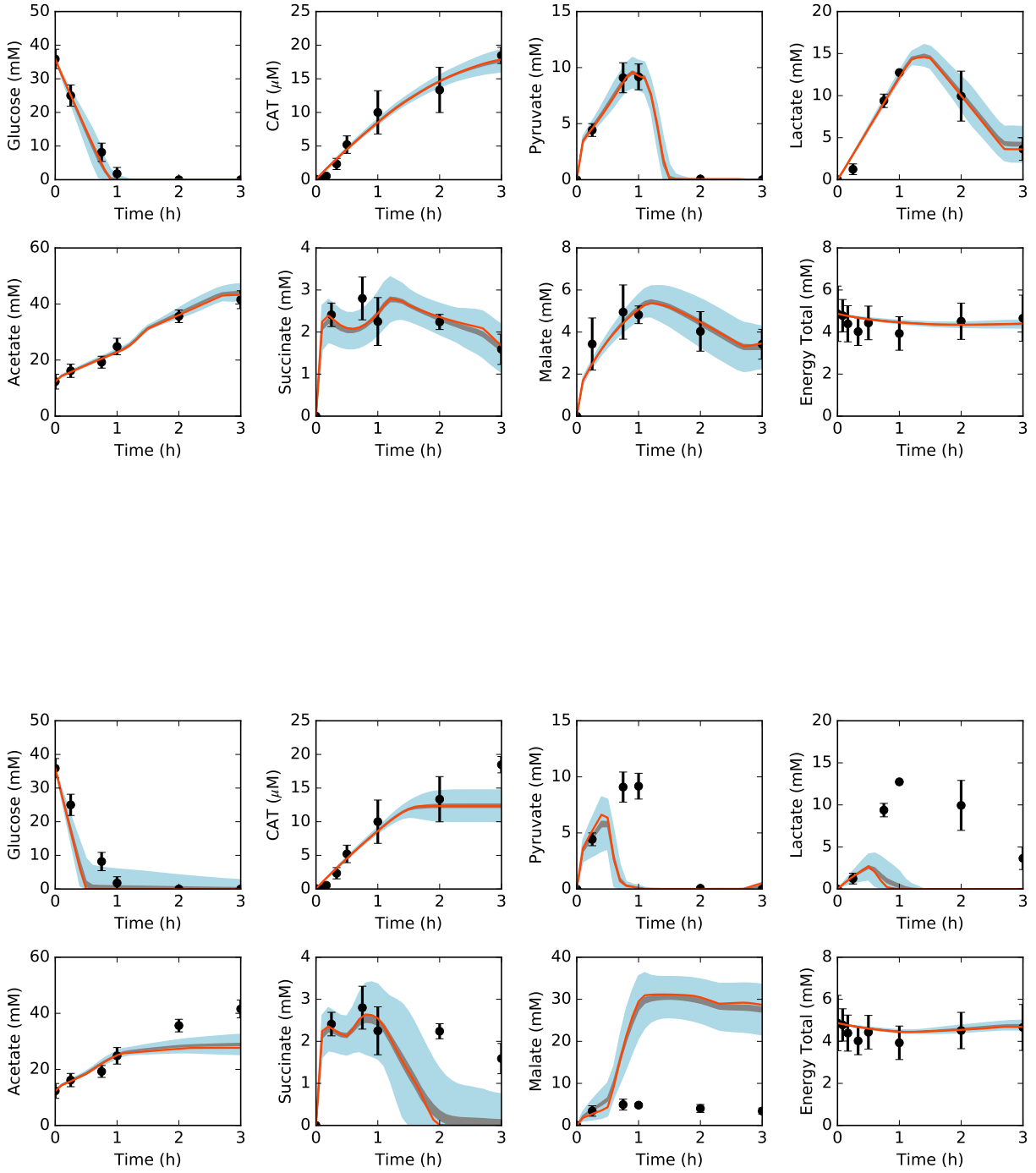


**Fig. 1:** Central carbon metabolism in the presence (top) and absence (bottom) of allosteric control, including glucose (substrate), CAT (product), and intermediates, as well as total concentration of energy species. Best-fit parameter set (orange line) versus experimental data (points). 95% confidence interval (blue shaded region) and 95% confidence interval of the mean (gray shaded region) over the ensemble of 100 sets.

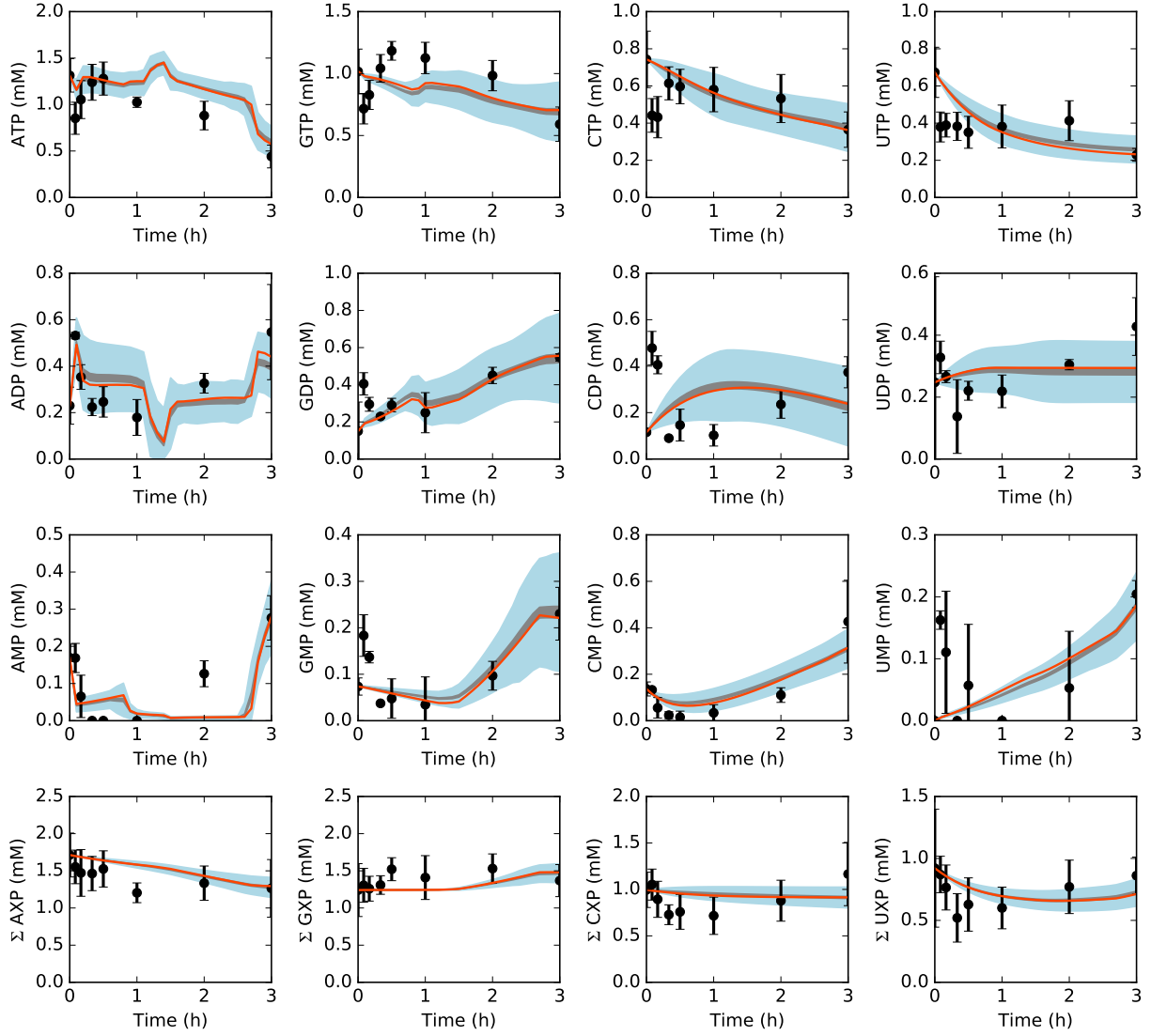


**Fig. 2:** Energy species and energy totals by base in the presence of allosteric control. Best-fit parameter set (orange line) versus experimental data (points). 95% confidence interval (blue shaded region) and 95% confidence interval of the mean (gray shaded region) over the ensemble of 100 sets.

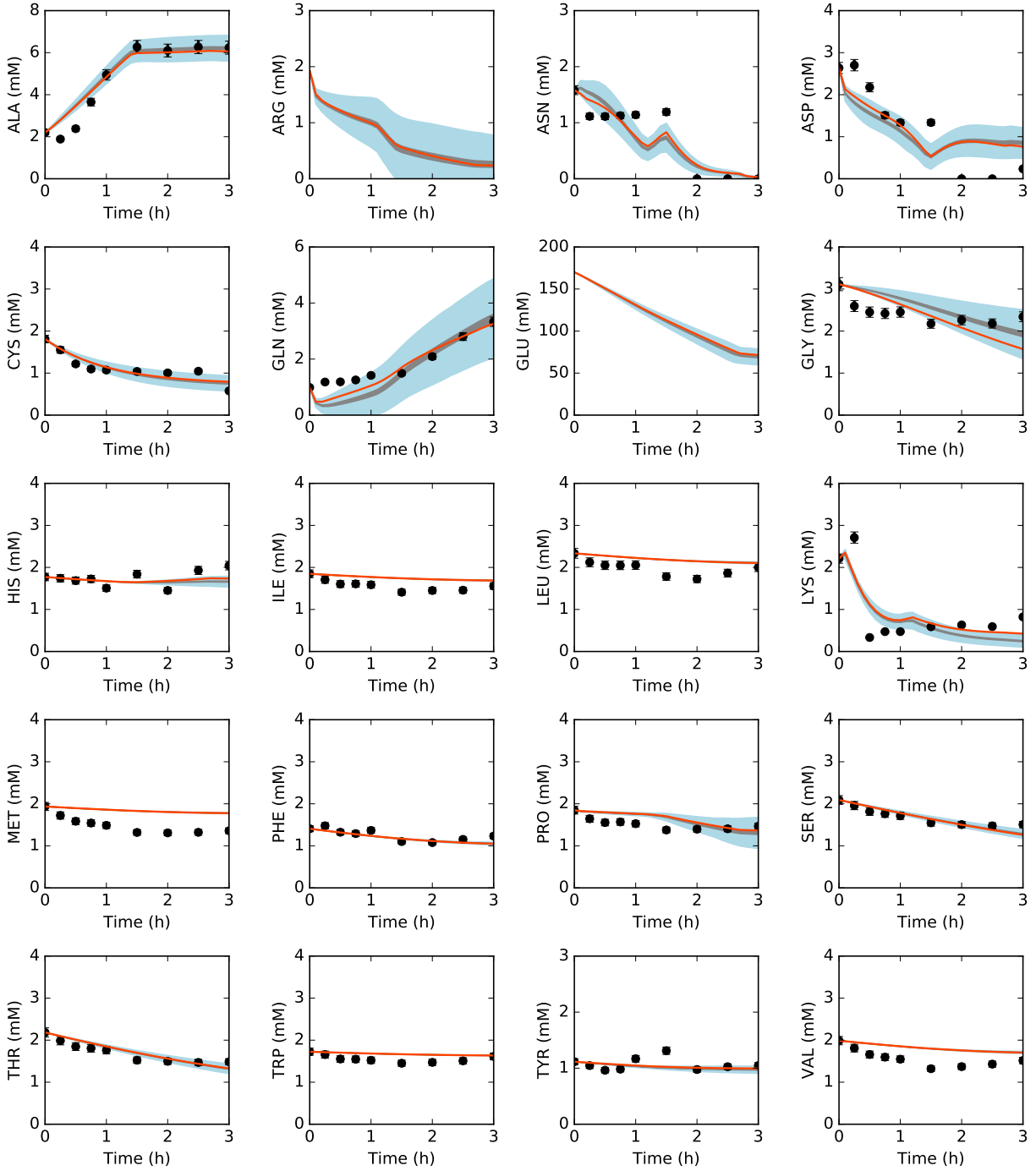


**Fig. 3:** Amino acids in the presence of allosteric control. Best-fit parameter set (orange line) versus experimental data (points). 95% confidence interval (blue shaded region) and 95% confidence interval of the mean (gray shaded region) over the ensemble of 100 sets.

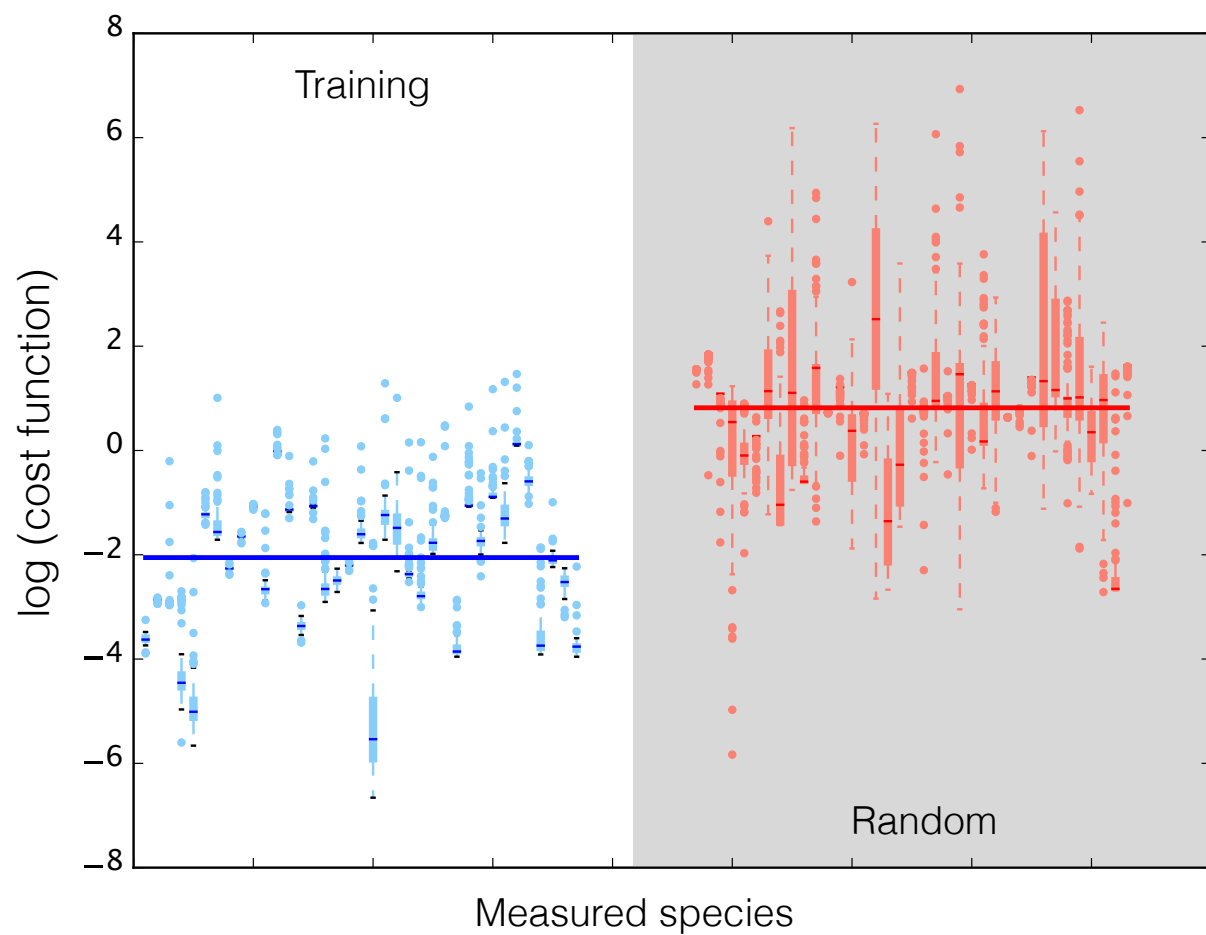


**Fig. 4:** Log of cost function across 37 datasets for data-trained ensemble (blue) and randomly generated ensemble (red, gray background). Median (bars), interquartile range (boxes), range excluding outliers (dashed lines), and outliers (circles) for each dataset. Median across all datasets (large bar overlaid).

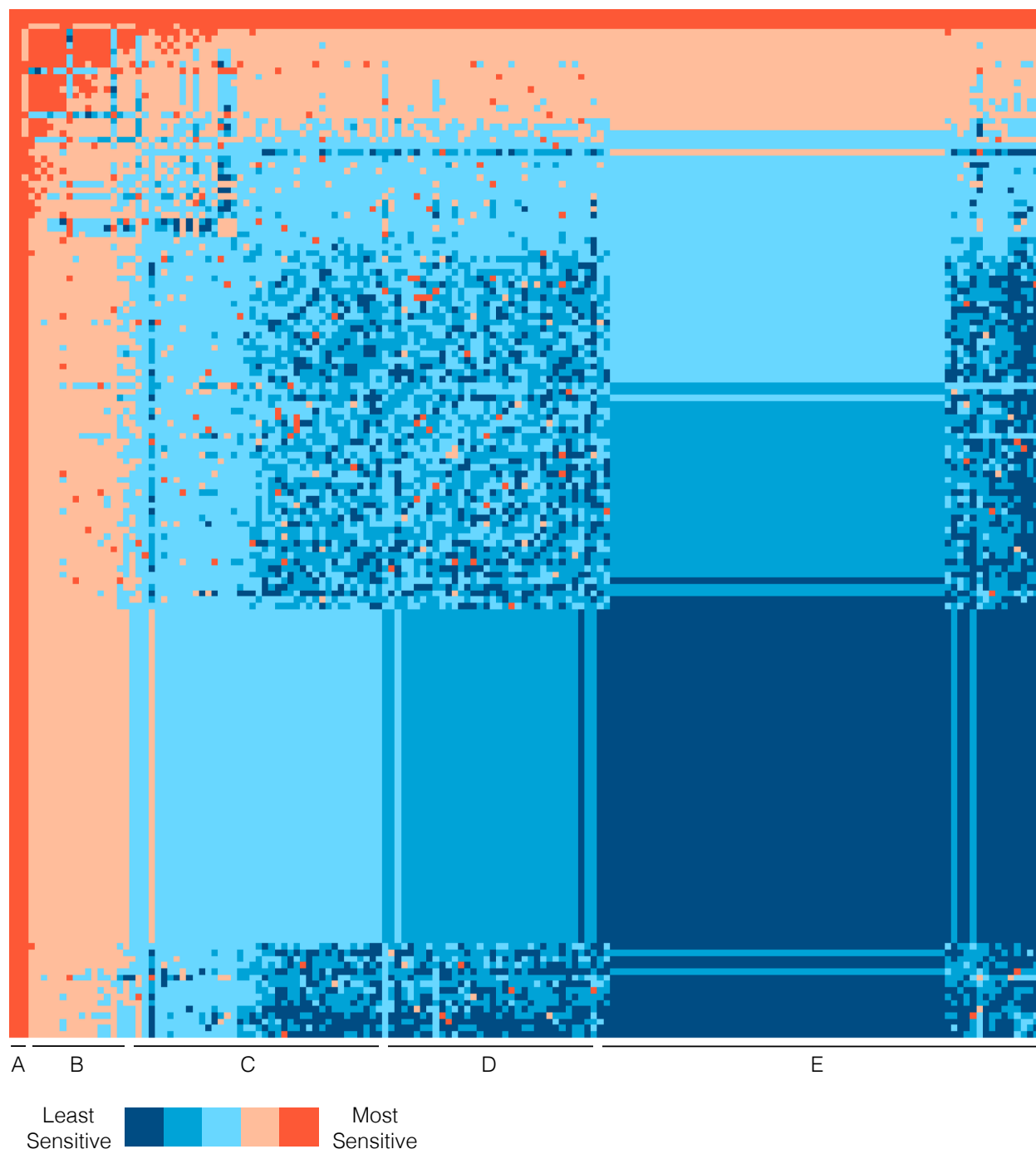


**Fig. 5:** Normalized first-order and pairwise sensitivities of CAT production to rate constants.

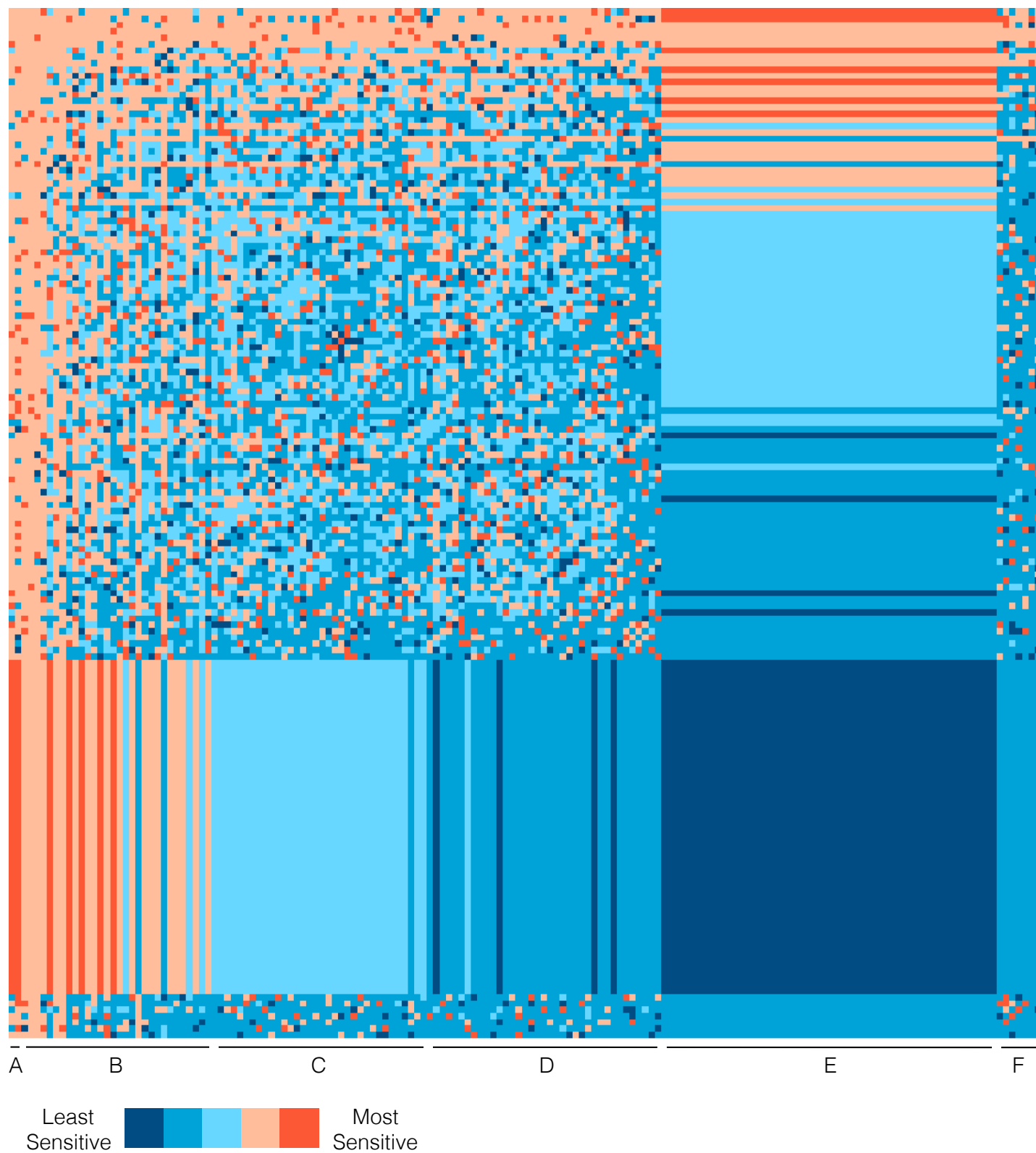


**Fig. 6:** Normalized first-order and pairwise sensitivities of system state to rate constants. A (most sensitive parameters): hexokinase run by GTP, and lactate dehydrogenase forward reaction. B:

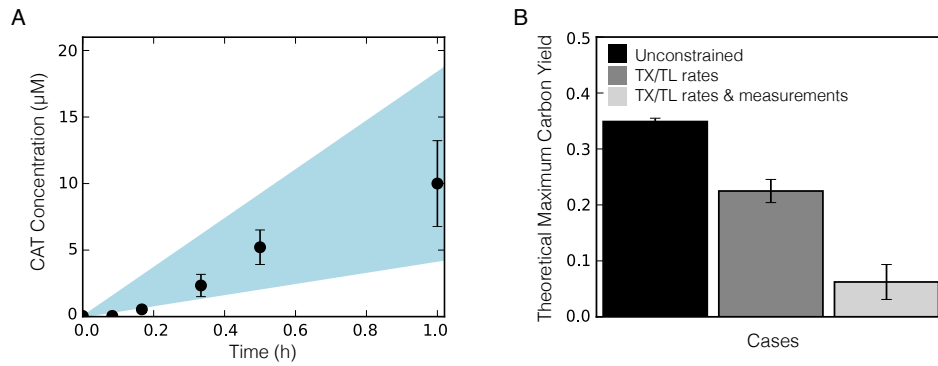


**Fig. 7:** Sequence specific flux balance analysis of CAT production and yield. **A.** 95% confidence interval of the ensemble (light blue region) for CAT concentration versus time. **B.** Theoretical maximum carbon yield of CAT calculated by ssFBA for three different cases: unconstrained except for glucose uptake (black), constrained by transcription and translation rates (grey), and constrained by transcription, translation rates and experimental measurements where available (light grey). Error bars represent standard deviation of the ensemble.

